CGI2012 manuscript No.
(will be inserted by the editor)

Complex Line Bundle Laplacians

Alexander Vais · Benjamin Berger · Franz-Erich Wolter

May 18, 2012

Abstract In the present work we extend the theoretical and numerical discussion of the well-known Laplace-Beltrami operator by equipping the underlying manifolds with additional structure provided by vector bundles. Focusing on the particular class of flat complex line bundles, we examine a whole family of Laplacians including the Laplace-Beltrami operator as a special case.

To demonstrate that our proposed approach is numerically feasible, we describe a robust and efficient finite-element discretization, supplementing the theoretical discussion with first numerical spectral decompositions of those Laplacians.

Our method is based on the concept of introducing complex phase discontinuities into the finite element basis functions across a set of homology generators of the given manifold. More precisely, given an m-dimensional manifold M and a set of n generators that span the relative homology group $H_{m-1}(M, \partial M)$, we have the freedom to choose n phase shifts, one for each generator, resulting in a n-dimensional family of Laplacians with associated spectra and eigenfunctions. The spectra and absolute magnitudes of the eigenfunctions are not influenced by the exact location of the paths, depending only on their corresponding homology classes.

Employing our discretization technique we provide and discuss several interesting computational examples highlighting special properties of the resulting spectral decompositions. We examine the spectrum, the eigenfunctions and their zero sets which depend continuously on the choice of phase shifts.

A. Vais · B. Berger · F.-E. Wolter
Welfenlab, Division of Computer Graphics
Leibniz University of Hannover, Germany
E-mail: {vais,bberger,few}@welfenlab.de

1 Introduction

The Laplace-Beltrami operator was first introduced and considered in purely theoretical settings in order to adapt the well-known Euclidean Laplacian to the realm of smooth manifolds. Typically it is defined to act on real-valued scalar functions f by $\Delta f = d^* df$ where d is the differential and d^* its adjoint.

Since manifolds provide a general setting for describing geometrical shapes, the feasibility of computable discretizations of the Laplace-Beltrami operator, see e.g. [5,7,42,37,24,1], has led to numerous applications in geometry processing algorithms, exploiting the close connection between the geometry of M and properties of the spectral decomposition of this operator. Computing the spectral decomposition of Δ amounts to solving the equation $\Delta f = \lambda f$ which results in an infinite sequence of real non-negative eigenvalues $\lambda_1, \lambda_2, \ldots$, called spectrum of Δ and a sequence of eigenfunctions $f_1, f_2, \ldots$ corresponding to the eigenvalues. Important features are its invariance under isometric deformations being a consequence of its purely intrinsic definition and its ability to capture geometric similarity in a compressed manner.

Among the known applications are shape and image retrieval using a prefix of the spectrum as a fingerprint or "Shape-DNA" [26,27,21,22]. For the apparently earliest reference to the latter application see [38], with details in [39]. A corresponding patent application was presented in [40]. Further applications are geometric signal processing operations [33,16,35], surface remeshing [6], creating descriptors for shape matching [30,32, 2,29,13,18], shape segmentation and registration [23, 14], statistical shape analysis for medical studies [28, 19,25] and symmetry detection[20], just to mention a few. A survey of some applications can be found in [43].

Along with the familiar concept of manifolds, the concept of vector bundles is a very natural construction in differential geometry and algebraic topology. Common geometrically motivated examples include the tangent and cotangent bundle. Bundles also provide a natural setting for studying differential operators and partial differential equations. However, while there is a great variety of other bundles that can be constructed, few concrete computational examples have been given so far.

Most of the above-mentioned works focus on the Laplace-Beltrami operator which can be interpreted as a Laplacian on the trivial vector bundle $M \times \mathbb{R}$. Recently [34] considered an approach for obtaining spectral decompositions for a class of Laplacian operators on non-trivial real line bundles over two-dimensional surfaces, introducing a global topological "twist" into the bundle $M \times \mathbb{R}$.

The contribution of the present work is to extend the above discussion by considering complex line bundles which offer significantly more flexibility for shapes with non-trivial topology. While the simplest complex line bundle $M \times \mathbb{C}$ does not give any new information compared to $M \times \mathbb{R}$, it can be modified in order to introduce a global twist analogously to the real-valued case.

The twisting in the real-valued case is determined by a choice of signs, yielding a finite number of distinct bundles with associated Laplacians. However, our newly proposed complex-valued approach allows for a continuum of phase parameters and accordingly many bundle Laplacians. The real-valued case is completely covered by choosing the phase parameters as integer multiples of π. However, there is a rich variety of Laplacians corresponding to other parameter choices, leading to spectral properties which cannot be obtained from a real-valued approach. All considered Laplacians only depend on intrinsic quantities and are therefore invariant under isometric deformations.

Introducing the concept of a connection and its associated curvature, it is possible to speak of flat bundles and it turns out that even the special case of flat complex line bundles considered here already offers a rich structure. Our current contribution can also be seen as a first step towards a numerical approach for considering Laplacians also on non-flat complex line bundles.

To substantiate the theoretical discussion with concrete computational examples, we focus first on the two-dimensional case and propose a discretization method. We also include first three-dimensional examples indicating our approach to be generalizable to higher dimensions.

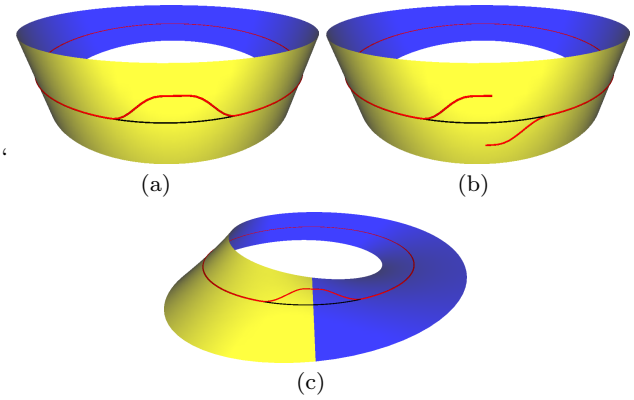

Fig. 1 (a) Graph of a smooth real-valued function (red) over the circle (black) interpreted as a section of the trivial bundle. (b) Introduction of a sign-flip discontinuity. (c) By going to the twisted bundle, the graph becomes continuous again.

2 Geometric Background

Roughly spoken, our approach is based on forcing any function on the surface to have a complex phase shift across a specific set of paths lying on the surface. This is accomplished by modifying the standard finite element basis functions accordingly.

At first one might think that an artificial introduction of discontinuities would produce results that depend on the precise choice of paths, or in the worst case, to produce no results at all as the finite element method for the Laplacian eigenvalue problem is typically formulated in terms of continuous basis functions. However, it turns out that the results are invariant with respect to the choice of paths up to homology and that the theory of vector bundles provides the appropriate context for interpretation.

To give an intuitive picture of the main idea, consider a smooth function $f : S^1 \to \mathbb{R}$ over the circle S^1. We can draw its graph as a smooth curve on a cylinder as shown in fig. 1. Introducing a sign flip at a certain place $c \in S^1$ makes the graph discontinuous. However this discontinuity disappears if we cut up the cylinder at the vertical line centered at c and glue it back together after a twist. The result obtained is the Möbius band. On this object, the graph of the function f has become a smooth curve again and it seems reasonable to be able to differentiate it. The Laplace Beltrami operator on the circle is given locally by $\Delta = -\frac{d^2}{dt^2}$ with $t \in [0, 2\pi]$ being the arc-length parameter. Assuming that the cutting point c corresponds to $t = 0 \pmod{2\pi}$, computing the spectral decomposition amounts to solving the boundary value problem $-f''(t) = \lambda f(t)$ with antiperiodic boundary conditions. Note that this procedure does not depend essentially on where c is located.

Following this line of thought leads to the notion of vector bundles, an important concept in topology and differential geometry. Using this theoretical framework, the discontinuities explicitly present in the functions disappear when the functions are replaced by sections of an appropriately twisted vector bundle. In the following section we will briefly review this framework. We will also need some basics of algebraic topology in order to classify and construct different vector bundles, as briefly collected in Appendix A. A comprehensive treatment can be found in textbooks on differential geometry and topology such as [17,11].

2.1 Vector Bundles

Intuitively, a real (or complex) rank k vector bundle E over a manifold M is obtained by assigning to each point $p \in M$ a real (or complex) k-dimensional vector space E_p in a continuous way. The vector space E_p is called fiber over p. Vector bundles of rank one are called line bundles. For a formal definition of vector bundles, see e.g. [9].

The cylinder and the Möbius band in fig. 1 are examples for real line bundles over the circle $M = S^1$. In the first case, a copy of $\mathbb{R}$ is assigned to each point, resulting in a bundle $E = M \times \mathbb{R}$. The second case, while locally similar, is topologically different because of the global twist. A bundle having the structure of a global Cartesian product $M \times V$ for some vector space V is called trivial. However, not all vector bundles are trivial, as the Möbius band shows. Instead, they satisfy only a local Cartesian product condition: For each point there is a neighborhood U such that the bundle over U is homeomorphic to $U \times \mathbb{R}^k$ (or $U \times \mathbb{C}^k$). This is called a trivialization of the bundle over U. If V is another neighborhood, then one has a transition function $h_U \mapsto h_V$, that relates both trivializations via a linear isomorphism on the respective fibers, see fig. 2.

An important real rank m vector bundle associated to an m-dimensional manifold is its tangent bundle TM which is the collection of all tangent spaces. The cotangent bundle T^*M is the dual bundle of TM, consisting of the collection of all vector spaces being dual to the tangent spaces. For two-dimensional manifolds these bundles can be viewed either as real bundles of rank two or as complex line bundles.

A map $s : M \to E$ with the property that $s(p) \in E_p$ is called a section of E. The space of all smooth sections is denoted by $\Gamma(E)$. For example, a section of the trivial line bundle $M \times \mathbb{C}$ is just a function $f : M \to \mathbb{C}$. A section of the tangent bundle TM is a vector field. A section of the cotangent bundle T^*M is a differential one-form.

Often, vector bundles are equipped with additional structure, such as a metric or a connection: An Euclidean vector bundle is a real vector bundle which is equipped with a smoothly varying symmetric positive definite bilinear form $\langle \cdot, \cdot \rangle : E_p \times E_p \mapsto \mathbb{R}$ on its fibers, called fiber metric. The space of sections $\Gamma(E)$ of an Euclidean vector bundle $(E, \langle \cdot, \cdot \rangle)$ becomes a Hilbert space by introducing the scalar product

$$(\phi, \psi) := \int_M \langle \phi, \psi \rangle \; dM \; .$$

These constructions carry over to complex vector bundles using a Hermitean inner products instead of an Euclidean inner product. In this case one speaks of Hermitean vector bundles. Note that a Hermitean inner product is not symmetric. Instead we have $\langle u, v \rangle = \overline{\langle v, u \rangle}$ and therefore $(u, v) = \overline{(v, u)}$ where $\overline{z}$ denotes complex conjugation of $z \in \mathbb{C}$.

A differentiable manifold whose tangent bundle TM is equipped with a fiber metric is called Riemannian manifold. Generally, a metric on a bundle E induces a metric on the dual bundle E^*. Metrics on two bundles E_1, E_2 induce a metric in the product bundle $E_1 \otimes E_2$.

A connection ∇ on a vector bundle E is a differential operator $\nabla : \Gamma(E) \to \Gamma(E \otimes T^*M)$ that satisfies the Leibniz rule

$$\nabla(fs) = s \otimes df + f \nabla s \quad f \in C^\infty(M), s \in \Gamma(E).$$

Here d denotes the exterior derivative or differential which maps functions (zero-forms) to one-forms. A connection can be considered as an extension of this concept, mapping from the space of E-sections (E-valued zero-forms) to the space of E-valued one-forms. Those spaces are equipped with inner products induced by those on E and on TM.

A connection is called flat if its associated curvature, see [17] vanishes. Bundles equipped with a flat connection are called flat. Note that the exterior derivative on functions can be considered as a flat connection on the trivial line bundle over M.

2.2 Connection Laplacians

Given an Euclidean or Hermitean vector bundle E with a connection ∇, the adjoint of ∇ is denoted by the map

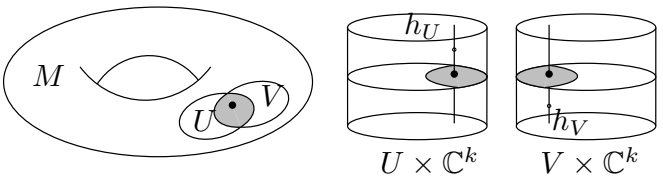

Fig. 2 Local Cartesian product structure of vector bundles.

$\nabla^* : \Gamma(E \otimes T^*M) \to \Gamma(E)$. Using the connection and its adjoint, the Connection Laplacian associated to ∇ is defined by

$$\Delta := \nabla^*\nabla : \Gamma(E) \to \Gamma(E)$$

The well-known Laplace-Beltrami operator $\Delta = d^*d$ arises as a special case of this general construction. We will exploit this point of view in order to construct Laplacian operators on flat complex line bundles and to study their properties numerically.

2.3 Classification of Line Bundles

Considering the variety of possible line bundles, the question of classification arises naturally. Let E_1, E_2 be two vector bundles over M. A vector bundle isomorphism is a homeomorphism $\phi : E_1 \to E_2$ that maps the fiber $E_1|_p$ to the fiber $E_2|_p$ via a linear isomorphism.

Up to vector bundle isomorphisms, real line bundles over a manifold are classified by elements of the first cohomology group $H^1(M, \mathbb{Z}_2)$, while complex line bundles are classified by elements of the second cohomology group $H^2(M, \mathbb{Z})$.

Note that for the circle $M = S^1$ this implies that there are exactly two real line bundles up to isomorphism, the non-trivial one being given by the Möbius band example. However, any complex line bundle over the circle is trivial, since the second cohomology group of the circle vanishes.

For a closed orientable surface M of genus g the first cohomology group has rank $2g$ so there are 2^{2g} different real line bundles up to isomorphism. Embedding these bundles in the complex setting, they become topologically equivalent as they all correspond to the zero cohomology class in $H^2(M, \mathbb{Z})$. However, there is a whole continuum of topologically equivalent bundles containing those 2^{2g} bundles, each giving rise to its own bundle Laplacian.

For surfaces with boundary H^2 vanishes, but for closed surfaces there is a countable number of topologically distinct complex line bundles, since $H^2(M, \mathbb{Z}) \cong \mathbb{Z}$. In this work we focus on the zero class.

3 Description of our Approach

In the following, we assume M to be a two-dimensional surface. Later on we will briefly indicate that it is possible to extend the construction to higher dimensions. Let $c_1, \ldots, c_n$ be a set of loops which generate the first fundamental group $\pi_1(M)$ of M. Cutting the surface along the loops c_i yields a tile of the universal cover $\widetilde{M}$. Note that the surface can be recovered by a corresponding inverse gluing operation, i.e by identifying two points $\widetilde{p}, \widetilde{q}$ in the universal cover if they differ by the action of an element of $\pi_1(M)$ in the sense of fig. 12.

Let $E_1 = M \times \mathbb{C}$ be the trivial complex line bundle over M. It can be constructed from the trivial complex line bundle $\widetilde{M} \times \mathbb{C}$ over $\widetilde{M}$ by identifying $(\widetilde{p}, v)$ with $(\widetilde{q}, w)$ if $\widetilde{p}$ and $\widetilde{q}$ differ by the action of an element of $\pi_1(M)$ and if $v = w$.

Given a set of phase angles $\beta_1, \ldots, \beta_n$, one β_k for each generator c_k, we construct a second complex line bundle E_2 over M by identifying two points $(\widetilde{p}, v)$ and $(\widetilde{q}, w)$ in $\widetilde{M} \times \mathbb{C}$ if the points differ by the action of an element $c_{k_1} \cdots c_{k_r}$ of $\pi_1(M)$ and if v and w differ by a complex phase of $\beta_{k_1} + \cdots + \beta_{k_r}$.

The natural connection $\nabla = d$ on E_1 lifts to a connection on the bundle $\widetilde{M} \times \mathbb{C}$ and induces a connection on E_2, which we will also denote by ∇. Our goal is to compute the spectral decomposition of the connection Laplacian $\nabla^*\nabla$ acting on sections of E_2.

Both E_1 and E_2 are topologically equivalent. If all phase angles β_k are integer multiples of π, the underlying real bundles obtained by the above construction using $\mathbb{R}$ instead of $\mathbb{C}$ are in general non-trivial. The main point is, that for non-zero phase angles the twisting introduced by the phase shifts gives rise to different Laplacians and different spectral information.

The construction above implies that we have an assignment of phase shifts to the loops c_k. By interpreting these loops as elements of the homology group $H_1(M)$, this assignment yields cohomology elements in $H^1(M)$. In order to localize the transitions described by those cohomology elements, we employ their duals γ_k with respect to Poincaré or Lefschetz duality. Roughly spoken, instead of accumulating a phase shift of β_k as we go around a loop c_k, we induce a sudden transition across the cycle $\gamma_k \in H_1(M, \partial M)$.

In order to obtain the spectral information, our algorithm proceeds in four steps:

1. Determine a basis $\gamma_1, \ldots, \gamma_n$ of the first relative homology group $H_1(M, \partial M)$.
2. Discretize the eigenvalue problem $d^*df = \lambda f$ using finite element basis functions that have phase discontinuities β_k across the generators γ_k determined in the first step.
3. Solve the resulting complex generalized Hermitean eigenvalue problem with a numerical sparse solver.
4. Visualize the resulting spectra and eigenfunctions.

3.1 Computing Homology Generators

We assume that our manifold is furnished with a triangulation (V, E, F) where V is the set of vertices, $E \subset V^2$ is the set of edges and $F \subset V^3$ is the set of faces. The set of vertices together with the edges form a graph (V, E). The dual of this graph is obtained as the graph (F, E^*) where $E^* \subset F^2$ is given by all pairs of faces sharing an edge in E. In the following, we identify E and E^* with each other. The problem of computing cycles on surfaces has been researched before, see e.g. [36,8,3,4] and the references therein. For our purposes we apply the algorithm of Erickson and Whittlesey [8]:

1. Compute a spanning tree $T \subset E$ of the graph (V, E).
2. Compute a spanning tree $T^* \subset E^*$ of the dual graph (F, E^*) using only edges not occurring in T.
3. Compute the set L of all edges not occurring in T or T^*. Each edge $e \in L$ induces a cycle in T.

This algorithm yields a set of $2g$ cycles for a closed manifold of genus g. For manifolds with k boundary loops, the algorithm is modified by treating each boundary loop as an additional face and augmenting the resulting cycles with $k-1$ independent paths connecting distinct boundary loops.

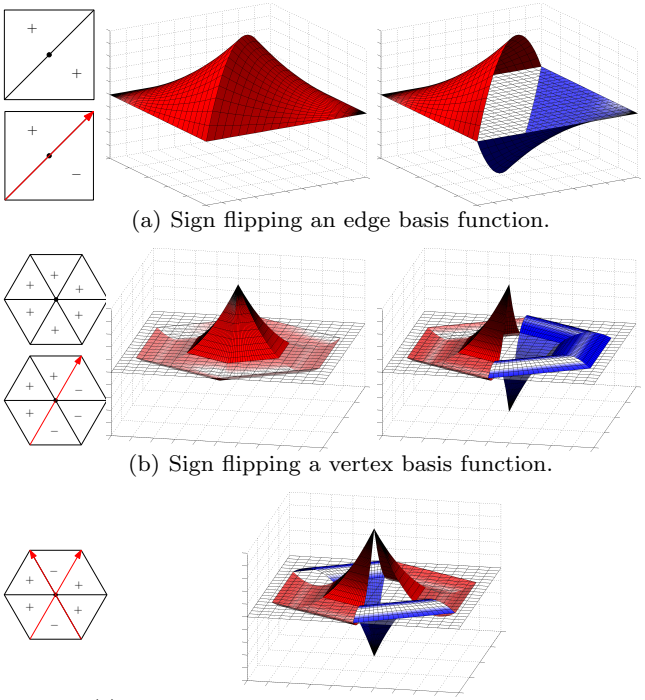

(a) Sign flipping an edge basis function.

(b) Sign flipping a vertex basis function.

(c) Double sign flipping a vertex basis function.

Fig. 3 Modified quadratic finite element basis functions in the real-valued case of phase shifts corresponding to sign flips.

3.2 Finite Element Formulation

The general outline for applying a finite element discretization to the Laplacian eigenvalue problem $d^*df = \lambda f$ is obtained in two steps: First, taking the inner product with an arbitrary test function φ we obtain the equation:

$$(d^*df, \varphi) = (df, d\varphi) = \lambda(f, \varphi) \quad \forall \varphi \ .$$

This weak variational formulation is discretized by writing the unknown function f as a linear combination $f = f^1\varphi_1 + \cdots f^N\varphi_N$ of a collection (φ_k) of suitable basis functions and solving the discrete generalized eigenvalue problem

$$Af = \lambda Bf \ ,$$

where A and B are $N \times N$ matrices and $f = (f^k)$ is a vector of dimension N. The entries of the matrices are computed by evaluating the inner products

$$A_{ij} = \int_M \langle d\varphi_i, d\varphi_j \rangle \ dM, \quad B_{ij} = \int_M \varphi_i \, \overline{\varphi_j} \ dM \ .$$

Notice that a complex conjugation of the second factor is present in the evaluation of these integrals in order to accommodate for the potentially complex valued basis functions φ_i.

According to standard finite element constructions, see e.g. [31], the basis functions are constructed by piecing together polynomials over the individual triangles in a triangulation of M to yield functions with local support that satisfy the interpolation conditions $\varphi_i(q_j) = \delta_{ij}$ on a set of N nodes (q_k) spaced regularly at the vertices, on the edges and in the interior of the triangles. This establishes a one-to-one correspondence between every node q_k and the basis function φ_k evaluating to one precisely at that node and to zero at all other nodes. Depending on where q_k is located, the corresponding basis function is called a vertex, edge or bubble function, respectively.

For the classical Laplace-Beltrami eigenvalue problem, the basis functions are real-valued and continuous. In our method we modify the basis functions to be complex-valued and to have a phase discontinuity across the set of homology generators computed in the previous section. Of course, these discontinuities reflect the twisting of the bundle. More precisely, any basis function whose support is crossed by one or more generators is affected. We will denote the generators as $\gamma_1, \ldots, \gamma_n$ and the corresponding phase angles by $\beta_1, \ldots, \beta_n$. Depending on the type of basis function we have three cases to consider:

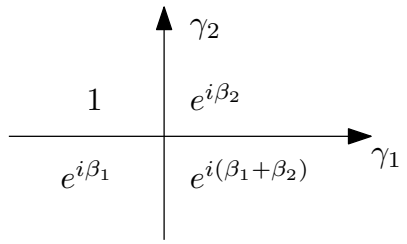

Fig. 4 Accumulation of phase shifts in the presence of multiple generators.

Bubble functions are not affected since their support is constrained to one triangle and they vanish on the edges of the triangle.

An edge basis function has a support consisting of two triangles. Assuming that some generator γ_k passes through the common edge and denoting by T_R the triangle on the right-hand side of γ_k, we multiply the values of the standard basis function over T_R with the factor $e^{i\beta_k}$.

A vertex basis function has a support consisting of all triangles incident to a vertex v. Assuming that a single generator γ_k passes through v, it divides the triangle fan into two sets T_L and T_R corresponding to the triangles to the left and to the right of γ_k. We apply a phase shift by multiplying the values of the standard basis function over T_R with the factor $e^{i\beta_k}$. If more than one generator passes through v, the modifications are accumulated by multiplication as shown in fig. 4.

In case of a phase of $\beta_k = \pi$ corresponding to a a sign flip, fig. 3 illustrates the modified quadratic edge and basis functions, showing only the real component as the imaginary component is zero. For phases β_k which are not integer multiples of π, the modified basis function become complex-valued with a non-zero imaginary component. In this case the matrix entries A_{ij} and B_{ij} have to be evaluated using the Hermitean inner products which amounts to using complex arithmetic and taking care of the conjugation of the second factor.

Note that our computations work with linear finite elements requiring only vertex basis functions as well as with higher order elements that require edge and bubble functions. The latter can be employed if high accuracy is desired.

3.3 Solving The Discrete Eigenvalue Problem

The resulting matrices A and B define a generalized Hermitean eigenvalue problem, in which A and B are Hermitean and B is positive definite. There are two possibilities to deal with the complex case: Either use a solver with complex arithmetic or reduce the problem to a real-valued symmetric eigenvalue problem with double dimension. The reduction is performed by assigning to a complex valued $n \times n$ matrix A a real valued $2n \times 2n$ matrix $\widetilde{A}$, replacing each entry z of A by a 2×2 block in $\widetilde{A}$: $z = x + iy \;\mapsto\; \left(\begin{smallmatrix} x & -y \\ y & x \end{smallmatrix}\right)$. Note that if A is Hermitean ($\overline{A^T} = A$) then $\widetilde{A}$ is symmetric ($\widetilde{A}^T = \widetilde{A}$). In our implementation we used the SLEPc library [12] with real arithmetic for solving the matrix eigenvalue problems.

4 Computations and Discussion

After having laid out the theoretical basics for the construction of a continuous family of flat complex bundle Laplacians, we continue with a discussion of several of their notable features in comparison to the Laplace-Beltrami operator. Therefore we employ the proposed finite element based discretization method in order to obtain numerical spectral decompositions for various geometric example shapes.

After focusing on the invariance properties of the construction, we describe how our approach provides a differentiable family of Laplacians containing the ordinary Laplace-Beltrami operator and compare the resulting spectra. Using an example we demonstrate how the eigenvalues of different bundle Laplacians adapt to geometric deformations in a predictable manner, showing that our method provides additional flexibility to supplement the data obtained from the Laplace-Beltrami operator. Afterwards, we focus on the resulting eigenfunctions and especially their characteristic zero sets. Finally we indicate that our construction can be generalized to a three-dimensional setting by giving first computational examples.

The spectral computations in our experiments are based on the following input data:

- A triangle mesh describing our manifold with or without boundary. We assume our mesh to be topologically correct.
- A set of paths $\gamma_1, \ldots, \gamma_n$ generating the first relative homology group. The paths can be obtained by the method in section 3.1.
- A set of phase angles β_k, one for each generator γ_k.

To visualize the resulting eigenfunctions we map the complex phase information to a cyclic color palette while an impression of the complex modulus is conveyed by tracing iso-lines. Note that for any eigenfunction f, the product cf for a constant $c \in \mathbb{C}$ is also an eigenfunction. By convention, the eigenfunctions are normalized to be orthonormal with respect to the Hermitean inner product which restricts c to have absolute value one. However, there remains an inherent phase ambiguity,

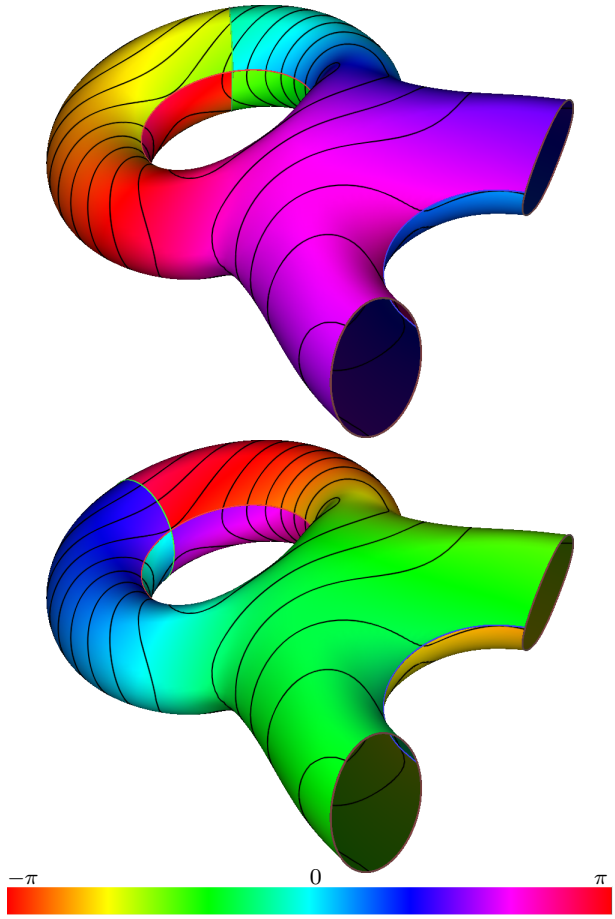

Fig. 5 Eigenfunction resulting from a phase shift of $\frac{\pi}{2}$ across all generators. The color palette indicates the complex phase while the contour lines show the complex amplitude which is a smooth function even across the generators. Changing the homology generator representatives only affects the phase information.

which can be irritating especially when comparing results in a series of computations. To resolve this ambiguity, we fix a common reference vertex and rotate all resulting eigenfunctions to become real-valued at that vertex.

4.1 Invariance

As an example shape with non-trivial topology we consider first a model of genus one with two boundary loops as shown in fig. 5. A set of paths generating the first relative homology group $H_1(M, \partial M)$ is given by the green handle loop γ_1, the red tunnel loop γ_2 and the blue path γ_3 connecting the two boundaries. For the spectral decomposition we applied Neumann boundary conditions on the two boundaries and phase shifts of $\beta_k = \frac{\pi}{2}$, $k = 1, 2, 3$ across all three paths. The plot shows the second eigenfunction.

We want to place emphasis on the fact that the results do not essentially depend on the specific choice of generators: Replacing a generator γ_k by a homologous generator γ_k' does not change the eigenvalue spectrum and also does not affect the absolute value (and therefore the corresponding contour lines) of the resulting eigenfunctions as shown in the bottom part of fig. 5. This is explained by the construction involving transitions of the form $e^{i\beta}$ which leave the modulus invariant.

4.2 Spectrum

If all phase angles are chosen as zero modulo 2π, we obtain the spectrum of the classical Laplace Beltrami operator. For a closed object, the spectrum starts with the eigenvalue zero, which corresponds to the constant function. However, introducing a non-zero phase shift makes the zero eigenvalue disappear since it is impossible for a locally constant function to satisfy the required phase jump.

To illustrate this behavior, consider the closed object of genus two shown in fig. 6. The red handle loop is one of the four generators that span the first homology group. We gradually increase the phase angle β across this loop from zero to π and plot the resulting first eigenfunctions while the evolution of the first few eigenvalues is shown in fig. 7. The constant eigenfunction gradually changes until it becomes real again for $\beta = \pi$. The corresponding eigenvalue zero rises to a positive eigenvalue.

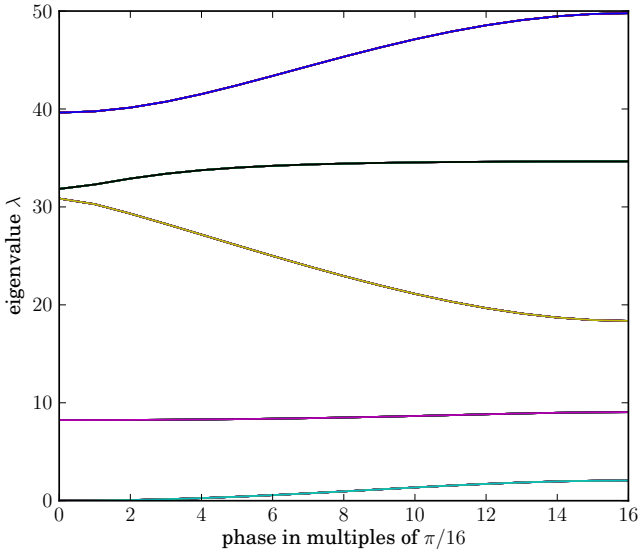

Fig. 7 Effect of continuously varying a phase between zero and π on the first eigenvalues for the double torus in fig. 6.

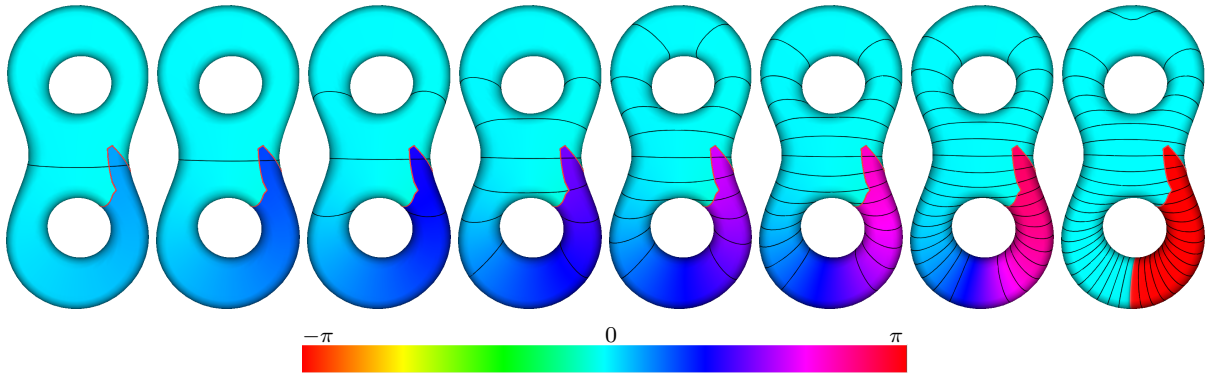

Fig. 6 Effect of continuously varying a phase between zero and π on the first eigenfunction. Each snapshot corresponds to a phase shift of $\frac{k\pi}{8}$ for $k = 1, \ldots, 8$ across the handle loop shown in red.

4.3 Modified Shape-DNA and HKS

As an application of the modified Laplacians for shape retrieval we suggest the extension of spectral-based concepts such as Shape-DNA [26,27], in which a prefix of the spectrum is used as a feature vector characterizing the shape. By varying our phase shift parameters β_k we are able to obtain different spectra that are more or less sensitive in response to specific shape deformations as indicated below.

As an example we created a smooth deformation of the genus one kitten model by thickening its tail over 30 time frames as shown in the top of fig. 8. The dimension of the homology group is two, spanned by a handle and a tunnel loop. Inducing a phase shift β across the handle loop creates a one-parameter family of bundles $E_H(\beta)$ and analogously we obtain a family $E_T(\beta)$ for phase shifts across the tunnel loop. We performed spectral decompositions of the corresponding Laplacians for each of the thirty kitten models and a sample of phases given by $\beta = k\frac{\pi}{16}$ with $k = 0, \ldots, 16$.

Figure 8 plots the distance between the resulting spectra and the classical Laplace-Beltrami spectrum obtained for the initial object. We have used the lowest 20 eigenvalues and the L^2 distance to perform the comparison of the spectra. Note that the deformation has almost no influence on the spectra obtained from $E_H(\beta)$, whereas it is clearly visible in $E_T(\beta)$. Moreover, as β increases from zero to π, the effect is amplified. Therefore the spectra of the tunnel loop Laplacians are more sensitive to the deformation.

This example indicates how geometric deformations are reflected differently in spectra of the modified bundle Laplacians. Obviously, the modifications also have impact on all shape descriptors that are derived from spectral information. Choosing different phase shift parameters offers versatile data containing the information obtained by the spectral decomposition of the Laplace-Beltrami operator and therefore our approach allows to extend previous approaches which depend on spectral data, such as Shape-DNA [27] or the Heat Kernel Signature [20].

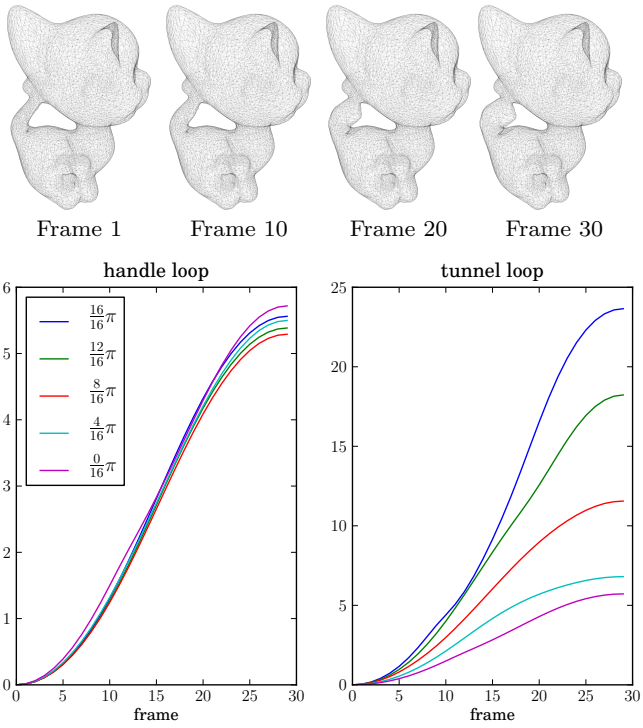

Fig. 8 Effect of a shape deformation on the spectra as measured by the L^2-distance from the Laplace-Beltrami spectrum of the undeformed object.

4.4 Zero Sets of Complex Eigenfunctions

We now shift our focus to the zero sets of the eigenfunctions. In contrast to the zero set of a regular real-valued function which is one-dimensional, the zero sets of our complex-valued eigenfunctions are in general zero-dimensional, consisting of isolated points. We remark,

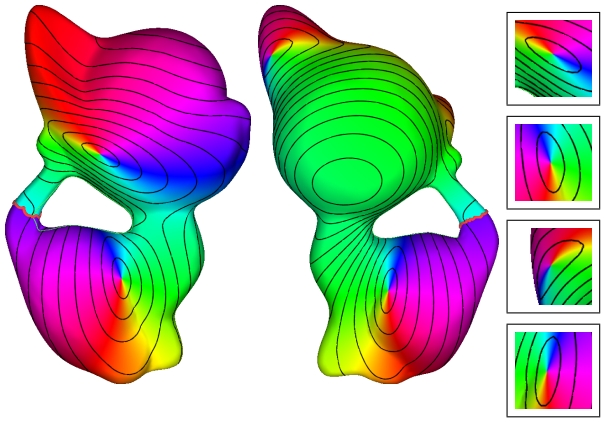

Fig. 9 Isolated zeros of a complex eigenfunction.

that the invariance of the contour lines with respect to the choice of homology generator representatives implies that the location of the isolated zeroes of any eigenfunction are characteristic for the intrinsic geometry of M and the concrete choice of phase shifts.

To each isolated zero p of f, the complex phase can be used to define the index of f at p, denoted by $\mathrm{ind}(f, p)$. This integer value intuitively captures the signed number of times that the phase rotates around that point. The index of a vector field $v \in \Gamma(TM)$ at a point p with $v(p) = 0$ is essentially the same concept.

According to a theorem of Chern, see e.g.[9], the sum of the indices of any section f of a complex line bundle E with a connection ∇ is a constant that can be computed by integrating the curvature of ∇ and which turns out to depend only on the topology of the bundle. Since we are dealing with flat line bundles this integral is zero. In fig. 9 we plotted an eigenfunction of the Laplacian corresponding to a phase shift of $\frac{\pi}{4}$ across the red loop around the tail of a kitten model. The two views show that there are four isolated zeros, two with index $+1$ and two with index -1. Their sum is zero, in accordance with the theory.

4.5 Zero Sets of Real Eigenfunctions

Returning to the real-valued case, notice that the one-dimensional zero set of the first eigenfunction corresponding to the phase $\beta = \pi$ in fig. 6 is a smooth curve that aligns well with a symmetry of the object and which lies in the same homology class as the handle loop that was used to induce the phase shift.

We performed several experiments with the zero sets of the first eigenfunctions and obtained results similar to [4] who compute cycles aligned with the principal curvature direction fields on the surface or [3] who compute short cycles that wrap around the handles and

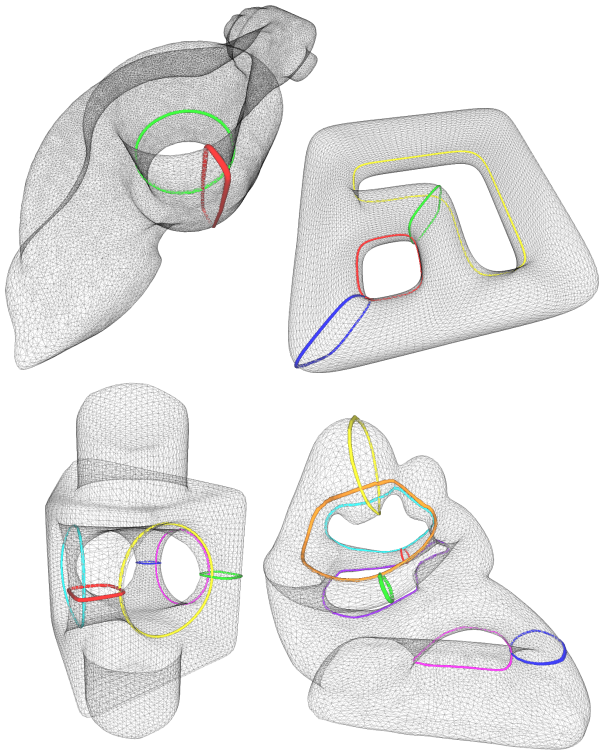

Fig. 10 Homology generators calculated from the zero sets of the first eigenfunctions.

tunnels of the surface. In our approach, we compute the zero sets of all 2^n first eigenfunctions corresponding to the phase shifts $\beta_1, \ldots, \beta_n \in \{0, \pi\}$ and sort these by total length. Then we pick out a set of n cycles that are linearly independent. Figure 10 shows the output of this method for objects of genus one to four. Note that these computations can also be obtained by using only real arithmetic, see [34].

The obtained zero sets form cycles that are characteristic for their respective homology classes and depend on the intrinsic properties of the surface. Therefore they can be used in the context of isometry invariant shape analysis for objects with non-trivial topology. An example application emphasizing the use of characteristic cycles in medical shape analysis can be found in [41].

4.6 Extension to Three Dimensional Solids

Up to now we focused our discussion on two-dimensional surfaces. The underlying theoretical framework discussed here allows the manifold in question to have any dimension, while the rank of the bundle remains one. In three dimensions we are dealing with volumetric objects and the sections of the considered complex line bundles can be modeled as functions that have phase dis-

continuities across some of the two-dimensional homology generators in $H_2(M, \partial M)$. Elements of this group can be pictured as equivalence classes of surfaces whose boundaries are contained in the boundary of M. The correspondence established above remains valid, i.e. the generator surface is homologous to any zero surface of a non-degenerate section of the constructed bundle. Especially it is homologous to the zero surface of the first eigenfunction, yielding smooth characteristic homology generator representatives.

Two computational examples are shown in fig. 11. In fig. 11(a) we generated a tetrahedral mesh for the two-dimensional double torus to yield a solid double torus. Its second relative cohomology group is two-dimensional and a generator has been computed using algebraic techniques. Inducing a phase shift of π yields the zero set of the first eigenfunction shown in red.

In fig. 11(b) a solid deformed torus has been carved out of a solid box. The second relative homology group is one-dimensional in this case. The representative obtained from the first eigenfunction is the red membrane clamped on the boundary of the torus.

We note that this three-dimensional extension of our approach could be useful in computing well-behaving surfaces generating the second relative homology group. These surfaces may serve as cuts for magnetic scalar potentials as considered for example in the works of Kotiuga [15,10].

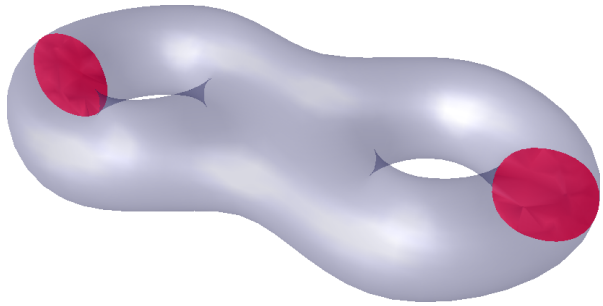

(a) Solid double torus.

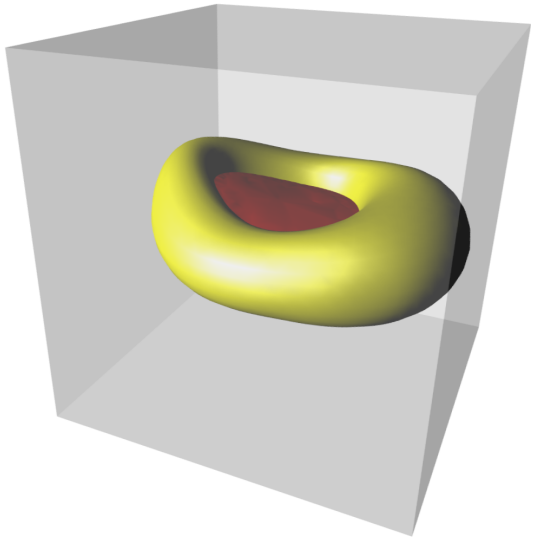

(b) Complement of a solid torus within a solid cube.

Fig. 11 Three-dimensional example

5 Conclusion and Outlook

In this paper we studied the numerical eigenvalue problem for flat complex line bundle Laplacians over a surface M. In this framework, the well-known Laplace-Beltrami operator $\Delta = d^*d$ acting on real-valued functions is identified with the bundle Laplacian acting on sections of the trivial real line bundle $M \times \mathbb{R}$. The underlying connection is the differential d that maps functions to differential one-forms.

This point of view leads naturally to a generalization in which we can study the problem of spectral computations for other connection Laplacians in the context of non-trivial real line bundles as well as complex line bundles.

The essence of the presented algorithm consists in discretizing the continuous eigenvalue problem using finite element basis functions that are modified by applying phase shifts across a set of paths that span the first relative homology group of the surface. Our method therefore is limited to surfaces with non-trivial topology as measured by the presence of handles or multiple boundaries. A surface is represented by a piecewise linear or smooth triangulation that carries the construction of the finite element basis functions. The homology generators we choose are paths along the edges of the triangulation. Following the standard Galerkin discretization leads to a sparse generalized Hermitean eigenvalue problem that can be solved using available software packages.

An important special case of our approach arises if the phase shifts are chosen as integer multiples of π, corresponding to sign flips across the generators. This yields the same results as previously introduced in [34] which features real-valued eigenfunctions that can be interpreted as sections of generally non-trivial real line bundles. However, by continuously varying the phase from zero to π, we can create a smooth transition from the classical Laplace-Beltrami operator on the trivial real line bundle to the aforementioned Laplacian operators acting on sections of non-trivial real line bundles.

While in this work we have focused on computational aspects, exploring the full range of geometry processing applications remains a topic for further research. It should be emphasized in this context, that the spec-

tra of the considered Laplacians and certain features that can be derived from their eigenfunctions, such as the zero sets, depend on the intrinsic geometry and are invariant with respect to the choice of homology generator representatives. The precise location of the homology generators on the surface is immaterial as predicted by the theory and confirmed by the numerical results. First examples indicating the applicability of our approach include the computation of intrinsic characteristic cycles and the extension of classical shape descriptors such as Shape-DNA and the heat kernel signature, considering the phase shifts as a newly available tool giving these applications more flexibility according to topological considerations.

Another topic for further research is the extension of the presented concepts to non-flat and non-trivial complex line bundles, noting that the tangent bundle and cotangent bundle provide natural examples.

Based on the first examples we expect our method to adapt also to topologically more challenging three-dimensional situations.

Acknowledgments

The authors would like to thank H. Thielhelm for valuable comments and suggestions. We also thank the AIM@SHAPE Repository for making accessible the 3D models used in this paper.

Appendix A: Algebraic Topology

Let M be a path-connected topological space. A continuous map $\gamma : [0,1] \to M$ with $\gamma(0) = \gamma(1) = p$ is called a loop with base point p. Two loops are called homotopic if one can be gradually deformed into the other. The set of equivalence classes of loops with a fixed base point is called the first fundamental group of M, denoted by $\pi_1(M,p)$.

A covering of M is a space $\widetilde{M}$ with a surjective local homeomorphism $\rho : \widetilde{M} \to M$. If $\widetilde{M}$ is simply connected, then ρ is called a universal covering of M. A deck transformation is a homeomorphism $h : \widetilde{M} \to \widetilde{M}$ such that $\rho \circ h = \rho$. Using these notions, another geometric interpretation of the first fundamental group is given by the fact that it is isomorphic to the deck transformation group of the universal cover of M.

To visualize this construction, consider a topological torus $M = S^1 \times S^1$ as shown in fig. 12. Its fundamental group is generated by two loops, denoted by a and b. Cutting the torus along these loops creates a rectangle, a so-called fundamental domain. The universal covering is the Euclidean plane $\widetilde{M} = \mathbb{R}^2$, which is tiled with

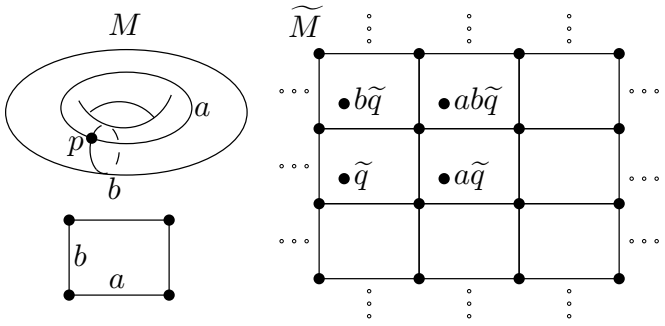

Fig. 12 Fundamental group of the torus acting on its universal covering space by deck transformations.

copies of the fundamental domain. The fundamental group acts on the points $\widetilde{q} \in \widetilde{M}$ by translation, sending $\widetilde{q}$ to the corresponding point in another copy of the fundamental domain.

Now, assume M is a manifold represented by a singular simplicial complex and let R be an arbitrary ring. A k-chain is a formal linear combination of oriented k-simplices with coefficients in the ring R. The set of k-chains form a group C_k under addition. The boundary operator $\partial_k : C_k \to C_{k-1}$ is a linear operator that maps any oriented simplex to the chain consisting of its appropriately signed oriented boundary simplices. A chain $\alpha \in C_k$ is called closed, or cycle, if $\partial\alpha = 0$ and it is called exact if it can be written as $\alpha = \partial\gamma$ for some $\gamma \in C_{k+1}$. Any exact chain is closed as a consequence of the fact that the boundary of a boundary is empty, i.e. $\partial^2 = 0$. Therefore, the sequence of chain groups C_k with the boundary operators in between form a chain complex.

Now let Z_k be the group of closed k-chains and let B_k be the group of exact k-cycles. Two cycles $\alpha, \beta \in Z_k$ are called homologous, if $\alpha - \beta \in B_k$. The k-th homology groups are the quotient groups $H_k(M,R) := Z_k/B_k$ induced by this equivalence relation.

The set of homomorphisms from H_k to R form the k-th cohomology group $H^k(M,R)$.

For manifolds M with non-empty boundary ∂M we will also need the so called relative homology groups $H_k(M,\partial M)$ which are obtained by modifying the homology equivalence relation to treat any chain on the boundary as zero. In this relative homology two relative k-cycles a, β are called homologous if $\alpha - \beta = \partial\gamma + \delta$ for a $(k+1)$-chain γ and some k-chain δ contained in the boundary ∂M.

The well-known Lefschetz duality theorem guarantees the existence of an isomorphism between the cohomology group $H^k(M)$ and the relative homology group $H_{m-k}(M,\partial M)$ where m denotes the dimension of the manifold.

For the annulus on the right the cycle α is a generator of $H_1(M)$. It is also a generator of the first fundamental group $\pi_1(M)$. The blue path β is not a cycle, since its boundary consists of two points. However it is a relative cycle since these points lie on the boundary ∂M. In fact β is a generator of $H_1(M, \partial M)$.

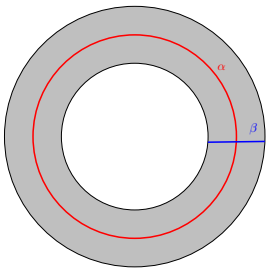

References

1. Alexa, M., Wardetzky, M.: Discrete Laplacians on General Polygonal Meshes. ACM TOG **30**(4), 102 (2011)
2. Bronstein, M.M., Kokkinos, I.: Scale-Invariant Heat Kernel Signatures for Non-Rigid Shape Recognition. In: Computer Vision and Pattern Recognition, pp. 1704–1711. IEEE (2010)
3. Dey, T.K., Li, K., Sun, J., Cohen-Steiner, D.: Computing Geometry-aware Handle and Tunnel Loops in 3D Models. ACM TOG **27**(3), 1–9 (2008)
4. Diaz-Gutierrez, P., Eppstein, D., Gopi, M.: Curvature Aware Fundamental Cycles. Computer Graphics Forum **28**(7), 2015–2024 (2009)
5. Dodziuk, J.: Finite-Difference Approach to the Hodge Theory of Harmonic Forms. American Journal of Mathematics **98**(1), 79–104 (1976)
6. Dong, S., Bremer, P., Garland, M., Pascucci, V., Hart, J.: Spectral Surface Quadrangulation. ACM TOG **25**(3), 1057–1066 (2006)
7. Dziuk, G.: Finite Elements for the Beltrami Operator on Arbitrary Surfaces. In: S. Hildebrandt, R. Leis (eds.) Partial Differential Equations and Calculus of Variations, *Lecture Notes in Mathematics*, vol. 1357, pp. 142–155. Springer Berlin / Heidelberg (1988)
8. Erickson, J., Whittlesey, K.: Greedy Optimal Homotopy and Homology Generators. In: Symposium on Discrete Algorithms, pp. 1038–1046. SIAM (2005)
9. Frankel, T.: The Geometry of Physics: An Introduction. Cambridge University Press (2011)
10. Gross, P.W., Kotiuga, P.R.: Electromagnetic Theory and Computation: A Topological Approach. Cambridge University Press (2004)
11. Hatcher, A.: Algebraic Topology. Cambridge University Press (2002)
12. Hernandez, V., Roman, J.E., Vidal, V.: SLEPc: A Scalable and Flexible Toolkit for the Solution of Eigenvalue Problems. ACM Transactions on Mathematical Software **31**(3), 351–362 (2005)
13. Hildebrandt, K., Schulz, C., von Tycowicz, C., Polthier, K.: Eigenmodes of Surface Energies for Shape Analysis. In: B. Mourrain, S. Schaefer, G. Xu (eds.) Advances in Geometric Modeling and Processing, *Lecture Notes in Computer Science*, vol. 6130, pp. 296–314. Springer (2010)
14. Hou, T., Qin, H.: Robust Dense Registration of Partial Nonrigid Shapes. IEEE Transactions on Visualization and Computer Graphics , preprint (2011)
15. Kotiuga, P.: An Algorithm to Make Cuts for Magnetic Scalar Potentials in Tetrahedral Meshes Based on the Finite Element Method. IEEE Transactions on Magnetics **25**(5), 4129–4131 (1989)
16. Lévy, B.: Laplace-Beltrami Eigenfunctions: Towards an Algorithm that Understands Geometry. International Conference on Shape Modeling and Applications (2006)
17. M. P. do Carmo: Riemannian Geometry. Birkhäuser Boston (1992)
18. Mémoli, F.: Spectral Gromov-Wasserstein Distances for Shape Matching. In: International Conference on Computer Vision, pp. 256–263 (2009)
19. Niethammer, M., Reuter, M., Wolter, F.-E., Bouix, S., Peinecke, N., Ko, M.S., Shenton, M.E.: Global Medical Shape Analysis using the Laplace-Beltrami-Spectrum. Medical Image Computing and Computer Assisted Intervention (2007)
20. Ovsjanikov, M., Sun, J., Guibas, L.: Global Intrinsic Symmetries of Shapes. Computer Graphics Forum **27**(5), 1341–1348 (2008)
21. Peinecke, N., Wolter, F.-E.: Mass Density Laplace-Spectra for Image Recognition. In: Cyberworlds, pp. 409–416. IEEE (2007)
22. Peinecke, N., Wolter, F.-E., Reuter, M.: Laplace-Spectra as Fingerprints for Image Recognition . Computer-Aided Design **39**(6), 460–476 (2007)
23. Reuter, M.: Hierarchical Shape Segmentation and Registration via Topological Features of Laplace-Beltrami Eigenfunctions. Journal of Computer Vision **89**, 287–308 (2010)
24. Reuter, M., Biasotti, S., Giorgi, D., Patanè, G., Spagnuolo, M.: Discrete Laplace-Beltrami Operators for Shape Analysis and Segmentation. Computers & Graphics **33**(3), 381–390 (2009)
25. Reuter, M., Niethammer, M., Wolter, F.-E., Bouix, S., Shenton, M.E.: Global Medical Shape Analysis using the Volumetric Laplace Spectrum. In: Cyberworlds, pp. 417–426. IEEE (2007)
26. Reuter, M., Wolter, F.-E., Peinecke, N.: Laplace-Spectra as Fingerprints for Shape Matching . In: Symposium on Solid and Physical Modeling, pp. 101–106 (2005)
27. Reuter, M., Wolter, F.-E., Peinecke, N.: Laplace-Beltrami Spectra as Shape DNA of Surfaces and Solids. Computer-Aided Design **38**(4), 342–366 (2006)
28. Reuter, M., Wolter, F.-E., Shenton, M.E., Niethammer, M.: Laplace-Beltrami Eigenvalues and Topological Features of Eigenfunctions for Statistical Shape Analysis. Computer Aided Design **41**(10), 739 – 755 (2009)
29. Ruggeri, M., Patanè, G., Spagnuolo, M., Saupe, D.: Spectral-Driven Isometry-Invariant Matching of 3D Shapes. Journal of Computer Vision **89**, 248–265 (2010)
30. Rustamov, R.M.: Laplace-Beltrami Eigenfunctions for Deformation Invariant Shape Representation. In: A. Belyaev, M. Garland (eds.) Symposium on Geometry Processing, pp. 225–233 (2007)
31. Solin, P.: Partial Differential Equations and the Finite Element Method. John Wiley & Sons (2005)
32. Sun, J., Ovsjanikov, M., Guibas, L.: A Concise and Provably Informative Multi-Scale Signature Based on Heat Diffusion. Computer Graphics Forum **28**(5), 1383–1392 (2009)
33. Taubin, G.: A Signal Processing Approach to Fair Surface Design. In: Computer Graphics and Interactive Techniques, pp. 351–358. ACM (1995)
34. Vais, A., Berger, B., Wolter, F.-E.: Spectral Computations on Nontrivial Line Bundles. Computers & Graphics **36**(5), 398–409 (2012)
35. Vallet, B., Lévy, B.: Spectral Geometry Processing with Manifold Harmonics. Computer Graphics Forum **27**(2), 251–260 (2008)

36. de Verdière, É.C., Lazarus, F.: Optimal System of Loops on an Orientable Surface. Discrete and Computational Geometry **33**(3), 507–534 (2005)
37. Wardetzky, M., Mathur, S., Kälberer, F., Grinspun, E.: Discrete Laplace Operators: No Free Lunch. In: Symposium on Geometry Processing, pp. 33–37 (2007)
38. Wolter, F.-E., Friese, K.-I.: Local and Global Geometric Methods for Analysis Interrogation, Reconstruction, Modification and Design of Shape. In: Computer Graphics International, pp. 137–151 (2000). Also available as Welfenlab report No. 3. ISSN 1866-7996.
39. Wolter, F.-E., Howind, T., Altschaffel, T., Reuter, M., Peinecke, N.: Laplace-Spektra - Anwendungen in Gestalt- und Bildkognition. Available as Welfenlab Report No. 7. ISSN 1866-7996.
40. Wolter, F.-E., Peinecke, N., Reuter, M.: Verfahren zur Charakterisierung von Objekten / A Method for the Characterization of Objects (Surfaces, Solids and Images). German Patent Application, June 2005 (pending), US Patent US2009/0169050 A1, July 2, 2009, 2006
41. Xin, S., He, Y., Fu, C., Wang, D., Lin, S., Chu, W., Cheng, J., Gu, X., Lui, L.: Euclidean Geodesic Loops on High-Genus Surfaces Applied to the Morphometry of Vestibular Systems. Medical Image Computing and Computer-Assisted Intervention–MICCAI 2011 pp. 384–392 (2011)
42. Xu, G.: Discrete Laplace-Beltrami Operators and their Convergence. Computer Aided Geometric Design **21**(8), 767–784 (2004)
43. Zhang, H., Van Kaick, O., Dyer, R.: Spectral Mesh Processing. Computer Graphics Forum **29**(6), 1865–1894 (2010)